

Haploinsufficiency of the Ammonia Transporter Rhcg Predisposes to Chronic Acidosis

Rhcg IS CRITICAL FOR APICAL AND BASOLATERAL AMMONIA TRANSPORT IN THE MOUSE COLLECTING DUCT*

Received for publication, December 3, 2012. Published, JBC Papers in Press, December 31, 2012, DOI 10.1074/jbc.M112.441782

Soline Bourgeois[‡], Lisa Bounoure[‡], Erik I. Christensen[§], Suresh K. Ramakrishnan^{¶||1}, Pascal Houillier^{¶||**‡‡}, Olivier Devuyst[‡], and Carsten A. Wagner^{‡2}

From the [‡]Institute of Physiology and Zurich Center for Integrative Human Physiology, University of Zurich, CH-8057 Zurich, Switzerland, the [§]Department of Biomedicine, University of Aarhus, 8000 Aarhus C, Denmark, [¶]INSERM, Centre de Recherche des Cordeliers, UMR5872, 75270 Paris, France, the ^{||}Faculté de Médecine, Université Pierre et Marie Curie, F-75015 Paris, France, the ^{**}Université Paris-Descartes, F-75015 Paris, France, and the ^{‡‡}Hôpital Européen Georges Pompidou, Département de Physiologie, Assistance Publique-Hôpitaux de Paris, F-75015 Paris, France

Background: Rhesus proteins transport NH₃ and/or NH₄⁺ in heterologous expression systems.

Results: Heterozygous Rhcg mice develop delayed metabolic acidosis, whereas homozygous KO mice display severe metabolic acidosis. RhCG functions as an NH₃ transporter on apical and basolateral membranes.

Conclusion: RhCG is an NH₃ but not NH₄⁺ transporter.

Significance: Loss or reduced expression of RhCG may underlie inherited or acquired forms of human acidosis.

Ammonia secretion by the collecting duct (CD) is critical for acid-base homeostasis and, when defective, causes distal renal tubular acidosis (dRTA). The Rhesus protein RhCG mediates NH₃ transport as evident from cell-free and cellular models as well as from *Rhcg*-null mice. Here, we investigated in a *Rhcg* mouse model the metabolic effects of Rhcg haploinsufficiency, the role of Rhcg in basolateral NH₃ transport, and the mechanisms of adaptation to the lack of Rhcg. Both *Rhcg*^{+/+} and *Rhcg*^{+/-} mice were able to handle an acute acid load, whereas *Rhcg*^{-/-} mice developed severe metabolic acidosis with reduced ammonuria and high mortality. However, chronic acid loading revealed that *Rhcg*^{+/-} mice did not fully recover, showing lower blood HCO₃⁻ concentration and more alkaline urine. Microperfusion studies demonstrated that transepithelial NH₃ permeability was reduced by 80 and 40%, respectively, in CDs from *Rhcg*^{-/-} and *Rhcg*^{+/-} mice compared with controls. Basolateral membrane permeability to NH₃ was reduced in CDs from *Rhcg*^{-/-} mice consistent with basolateral Rhcg localization. *Rhcg*^{-/-} responded to acid loading with normal expression of enzymes and transporters involved in proximal tubular ammoniogenesis but reduced abundance of the NKCC2 transporter responsible for medullary accumulation of ammonium. Consequently, tissue ammonium content was decreased. These data demonstrate a role for apical and basolateral Rhcg in transepithelial NH₃ transport and uncover an incomplete dRTA pheno-

type in *Rhcg*^{+/-} mice. Haploinsufficiency or reduced expression of RhCG may underlie human forms of (in)complete dRTA.

Ammonium (NH₄⁺) is the main component of urinary acid excretion. Renal synthesis and excretion of NH₄⁺ rise in response to an acid load, allowing kidneys to regenerate bicarbonate and increase net acid excretion (1, 2). Impaired renal acid excretion characterizes type I distal renal tubular acidosis (dRTA)³ with low urinary ammonium and inappropriately alkaline urinary pH (3).

Ammonium is formed in the proximal tubule from the metabolism of glutamine and added to the luminal fluid. It is reabsorbed into the medullary interstitium in the thick ascending limb creating a cortico-papillary NH₃/NH₄⁺ gradient (4, 5). The final step of NH₃/NH₄⁺ excretion is achieved by the CD (6). The high tissue concentration of NH₃/NH₄⁺ and the pH gradient between interstitium and urine provide the driving forces for NH₄⁺ excretion into urine. NH₄⁺ secretion results from the trapping of NH₃ in the tubular lumen after being titrated by H⁺ ions stemming from active secretion by V-type H⁺-ATPases (7).

The mechanisms mediating NH₃/NH₄⁺ transport across cell membranes into urine have only recently become uncovered. Members of the Rhesus protein family have been identified as pathways for NH₃/NH₄⁺ transport in yeast, plants, fish, and mammals (2, 5, 8). In the kidney CD, RhCG and RhBG are expressed (9, 10). Mice lacking *Rhbg* show either no phenotype or only a very mild reduction in urinary ammonium excretion (11, 12). In contrast, cell-specific or complete *Rhcg* deficiency

* This work was supported in part by Grants 3100A0-122217 and 31003A_138143 from the Swiss National Science Foundation (to C. A. W.), the 7th European Union Framework Project EUNEFRON (to P. H., E. I. C., O. D., and C. A. W.), the Danish Medical Research Council, The Novo Nordisk Foundation (to E. I. C.), and the Swiss National Centre of Competence in Research (to O. D. and C. A. W.).

¹ Supported by Erasmus Mundus External Cooperation Window Lot 15, India.

² To whom correspondence should be addressed: Institute of Physiology, University of Zurich, Winterthurerstrasse 190, CH-8057 Zurich, Switzerland. Tel.: 41-44-63-55023; Fax: 41-44-63-56814; E-mail: Wagnerca@access.uzh.ch.

³ The abbreviations used are: dRTA, distal renal tubular acidosis; CD, collecting duct; CCD, cortical CD; BCECF, 2',7'-bis(2-carboxyl)-5-(and-6)-carboxyfluorescein; PEPCK, phosphoenolpyruvate carboxylase; PDG, phosphate-dependent glutaminase; NMDG, *N*-methyl-D-glutamine; OMCD, outer medullary collecting duct; IMCD, inner medullary collecting duct.

causes a massive reduction in urinary ammonium excretion in three different mouse models (13–15). Microperfusion experiments using CDs from *Rhcg*-deficient mice demonstrated that RhCG is critical for the apical exit of NH_3 into urine (13). Thus far, a phenotype of dRTA has only been reported in *Rhcg*^{-/-} mice, whereas potential changes caused by haploinsufficiency in *Rhcg* have not been investigated. This issue is relevant because heterozygous abnormalities in RhCG might be more frequent and may affect the renal capacity to cope with an acid load leading to incomplete dRTA. Furthermore, *Rhcg*^{+/-} mice may also serve as a model to examine the consequences of reduced RhCG expression that may occur during kidney disease. Finally, RhCG localization has been controversial for years. RhCG has been localized by some groups only at the apical side of CD cells, whereas others have found RhCG on both the apical and basolateral membranes (9, 10, 16, 17). The functionality of basolateral RhCG protein remains unknown.

Here, we used a novel *Rhcg* mouse model to provide the first evidence that haploinsufficiency in *Rhcg* impairs the handling of a chronic acid load in *Rhcg*^{+/-} mice, which develop an incomplete metabolic acidosis. Microperfusion studies provide the functional basis of the defect and show that RhCG is absolutely required for apical and partially for basolateral NH_3 transport. Moreover, loss of *Rhcg* is associated with a profound down-regulation of NKCC2 and reduced medullary accumulation of ammonium impairing the gradient necessary for the final excretory step. These data provide new insights into the complex role of RhCG and suggest that congenital or acquired defects in *RhCG* protein expression may be associated with incomplete dRTA.

EXPERIMENTAL PROCEDURES

Animals—*Rhcg*^{+/-} mice were purchased from the Texas Institute of Genomic Medicine (Houston TX). Mice were generated by replacing exon 1 by a vector carrying a LacZ/Neo cassette (Fig. 1A). Mice were genotyped by PCR directly on a 3- μl 25 mM NaOH tail digestion product. Genomic DNA was amplified using primer pairs specific for exon 1 forward (AGACCCACAATGGAAAGCTATAA), wild type reverse (CAACCAGAACTCCCCAGTGTGAGA), and knock-out reverse (ATGGGCTGACCGCTTCCTCGTGCTTTAC). The products were separated by electrophoresis in 1% agarose gel (mutant product, 522 bp; wild type product, 376 bp). Mice were generated by mating *Rhcg*^{+/-} mice, and mice were bred in the Étres Vivants Exempts d'Organismes Pathogènes Spécifiques Animal Facility. For acid-loading experiments, mice in metabolic cages were given 0.2 M HCl added to powdered standard food. All experiments were performed according to Swiss Animal Welfare laws and approved by the local veterinary authority (Veterinäramt Zürich).

In Vivo Experiments—All experiments were performed using age- and sex-matched *Rhcg* wild type (*Rhcg*^{+/+}), *Rhcg* knock-out (*Rhcg*^{-/-}), and *Rhcg* heterozygote (*Rhcg*^{+/-}) littermate mice (3–4 month-old) that were housed in metabolic cages (Techniplast, Switzerland). Mice were given deionized water *ad libitum* and were fed with a standard powdered laboratory chow (Kliba, Augst, Switzerland). Mice were allowed to adapt to metabolic cages for 3 days, and a first retro-orbital blood

sample was taken for blood gas analysis under base line. Then two 24-h urine samples were collected under light mineral oil in the urine collector to determine daily urinary parameters. Mice were then allowed to recover for 2 weeks before giving an HCl-containing diet (0.2 M HCl added to powdered standard food) in normal cages. Food, water intake, and urine excretion were monitored following the same procedures as under base-line conditions. Urine collections were performed on the 1st and 2nd day of acid loading and then on the 6th and 7th day. Retro-orbital blood samples were taken on the 2nd and 7th days of HCl diet.

Analytic Procedures—Blood pH, pCO_2 , and electrolytes were measured with a pH/blood-gas analyzer (ABL 77 Radiometer). Urinary Na^+ and K^+ concentrations were measured by flame photometry (IL943, Instruments Laboratory); titratable acids were measured using a DL 50 titrator (Mettler Toledo) (18, 19) and creatinine by a modified kinetic Jaffé colorimetric method (20). Urinary pH and bicarbonate were measured with a pH/blood-gas analyzer (ABL 725, Radiometer). Urinary NH_4^+ was measured with the Berthelot protocol (21).

Immunoblotting—Crude membrane proteins or cytosolic fractions were obtained from kidneys homogenized in 250 mM sucrose, 10 mM Tris-HCl, pH 7.5, and in the presence of protease inhibitors.

Forty micrograms of crude membrane proteins or cytosolic proteins were solubilized in loading buffer containing DTT and separated on 8–10% polyacrylamide gels. For immunoblotting, the proteins were transferred electrophoretically to polyvinylidene fluoride membranes (Immobilon-P, Millipore Corp., Bedford, MA). After blocking with 5% milk powder in Tris-buffered saline, 0.1% Tween 20 for 60 min, the blots were incubated with primary antibodies overnight at 4 °C as follows: phosphate-dependent glutaminase (PDG), which recognizes both the rat (KGA) and human (GAC) kidney-type isoforms of PDG forming the mature PDG protein (66 and 68 kDa; a kind gift from N. Curthoys, Colorado State University; diluted 1:5000) (22); rabbit polyclonal anti-PEPCK (Cayman Chemical, Ann Arbor, MI; diluted 1:5000); rabbit polyclonal anti-NKCC2 (kind gift from Johannes Loffing, Institute of Anatomy, University of Zurich; diluted 1:5000); rabbit polyclonal anti-NHE3 (StressMarq Biosciences Inc., Victoria, British Columbia, Canada); rabbit polyclonal anti-pendrin (Pineda Antibody Service, Berlin, Germany, diluted 1:5000) (23); and mouse monoclonal anti- β -actin antibody (Sigma; diluted 1:5000). After washing and blocking with 5% milk powder for 60 min, membranes were then incubated for 2 h at room temperature with secondary goat anti-rabbit or donkey anti-mouse antibodies (diluted 1:5000) linked to alkaline phosphatase (Promega, Madison, WI). The protein signal was detected with the appropriate substrate (Millipore Corp, Bedford, MA) using the las-4000 image analyzer system (Fujifilm Life Science). All images were analyzed using the software Advanced Image Data Analyzer AIDA (Raytest, Straubenhardt, Germany) to calculate the protein of interest/ β -actin ratio.

Immunostaining and Immunogold—Immunohistochemistry and immunogold staining were performed on frozen sections, and specificity was demonstrated on *Rhcg*^{-/-} tissues. Mouse kidneys were fixed by perfusion retrograde through the aorta

Incomplete dRTA in Rhcg-targeted Mice

with 3% paraformaldehyde in 0.1 M sodium cacodylate buffer, pH 7.2. The tissue was either trimmed into small blocks, further fixed by immersion in 1% paraformaldehyde, infiltrated with 2.3 M sucrose for 30 min, and frozen in liquid nitrogen or prepared for routine paraffin embedding.

For electron microscopy, 70–90-nm cryosections were obtained at -100°C with an FCS Reichert Ultracut S cryoultramicrotome as described previously (24), and 2- μm paraffin sections were obtained with a Leica RM2165 microtome. For LM immunolabeling, the sections were incubated with a rabbit polyclonal antibody against RhCG (a kind gift from Dr. Yves Colin, INSERM, Paris, France (16, 25)) at room temperature for 1 h after preincubation in PBS containing 0.05 M glycine and 1% bovine serum albumin. The sections were subsequently incubated with peroxidase-conjugated secondary antibody (Dako); the peroxidase was visualized with diaminobenzidine, and the sections were counter-stained with Maier's stain for 2 min. The sections were examined in a Leica DMR microscope equipped with a Leica DFC320 camera. Images were transferred by a Leica TFC Twain 6.1.0 program and processed using Adobe Photoshop 8.0. For EM immunolabeling, the sections were incubated with the primary antibody at 4°C overnight followed by incubation at room temperature for 1 h with 10-nm gold particles coupled to anti-rabbit IgG (BioCell, Cardiff, UK). The cryosections were embedded in methylcellulose containing 0.3% uranyl acetate and studied under a Philips CM100 electron microscope. For controls, sections were incubated with secondary antibodies alone or with nonspecific IgG.

RNA Extraction and Reverse Transcription—Snap-frozen kidneys (five kidneys for each condition) were homogenized in RLT-Buffer (Qiagen, Basel, Switzerland) supplemented with β -mercaptoethanol to a final concentration of 1%. Total RNA was extracted from 200- μl aliquots of each homogenized sample using the RNeasy mini kit (Qiagen, Basel, Switzerland) according to the manufacturer's instructions. Quality and concentration of the isolated RNA preparations were analyzed on the ND-1000 spectrophotometer (Nano-Drop Technologies). Total RNA samples were stored at -80°C . Each RNA sample was diluted to 100 ng/ μl , and 3 μl was used as a template for reverse transcription using the TaqMan reverse transcription kit (Applied Biosystems, Foster City, CA). For reverse transcription, 300 ng of RNA template were diluted in a 40- μl reaction mix that contained (final concentrations) RT buffer (1 \times), MgCl_2 (5.5 mM), random hexamers (2.5 μM), RNase inhibitor (0.4 units/ μl), the multiscribe reverse transcriptase enzyme (1.25 units/ μl), dNTP mix (500 μM each), and RNase-free water.

Real Time Quantitative PCR—Quantitative real time quantitative RT-PCR was performed on the ABI PRISM 7700 sequence detection system (Applied Biosystems, Foster City, CA). Primers were chosen using the BLAST tool of Ensemble to result in amplicons no longer than 150 bp spanning intron-exon boundaries to exclude genomic DNA contamination. The specificity of all primers was first tested on mRNA derived from kidney and always resulted in a single product of the expected size (data not shown). Probes were labeled with the reporter dye 6-carboxyfluorescein at the 5' end and the quencher dye 5-(and 6)-carboxytetramethylrhodamine at the 3' end (Microsynth,

Balgach, Switzerland). The primers were designed to target the deleted sequence in *Rhcg*^{-/-} animals (accession number NM_019799) with 5'-ATGCAGGGATGGTTCCATTA-3' (238–258 bp) as the left primer located within exon 1 and 5'-TGGAAGAAGGTCATAATGAGCAG-3' (373–392 bp) as the right primer located within exon 2, and 5'-TTACTATCGCTACCCGAGCTTCCAG-3' as the probe (292–317 bp). Real time PCRs were performed using TaqMan Universal PCR master mix (Applied Biosystems, Foster City, CA). Briefly, 3 μl of cDNA, 0.8 μl of each primer (25 μM), 0.4 μl of labeled probe (5 μM), 5 μl of RNase-free water, and 10 μl of TaqMan Universal PCR master mix reached 20 μl of final reaction volume. Reaction conditions were denaturation at 95°C for 10 min followed by 40 cycles of denaturation at 95°C for 15 s and annealing/elongation at 60°C for 60 s with auto ramp time. All reactions were run in triplicate. For analyzing the data, the threshold was set to 0.2 as this value had been determined to be in the linear range of the amplification curves for all mRNAs in all experimental runs. The expression of the genes of interest was calculated in relation to hypoxanthine-guanine phosphoribosyltransferase (accession number NM_013556, forward primer, 5'-TTATCAGACTGAAGAGCTACTGTAAGATC-3' (442–471), reverse primer, 5'-TTACCAGTGTCAATTATATCTTCAACAATC-3' (539–568), and probe, 5'-TGAGAGATCATCTCCACCAATAACTTTTATGTCCC-3' (481–515)). Relative expression ratios were calculated as $R = 2^{-(Ct(\text{HPRT}) - Ct(\text{test gene}))}$, where *Ct* represents the cycle number at the threshold 0.02; and HPRT is hypoxanthine-guanine phosphoribosyltransferase.

Measurement of Renal Ammonia Content—The renal tissue ammonia content was measured by an enzymatic technique (ammonia assay kit, Sigma) as described previously (26). Mice were anesthetized, and the kidneys were removed and immediately frozen in liquid nitrogen. They were then sliced frozen to yield a column of tissue, which extended from the cortex to the tip of the papilla. Sections were cut along the corticomedullary axis to yield three slices as follows: cortex, outer medulla, and inner medulla. Two kidneys from the same animal were pooled for each sample. Tissue slices were then homogenized in 300 μl of ice-cold 7% trichloroacetic acid, and the solution was centrifuged. The supernatant was drawn off, and the pH of a 250- μl sample was adjusted to near neutral by the addition of 12 μl of 10 mM Na_2HPO_4 in 9 N NaOH. A 200- μl sample of buffered supernatant was then analyzed for ammonium. The pellet was resuspended in 1 N NaOH, shaken overnight, and analyzed for total protein using the Bio-Rad protein assay.

Microperfusion Studies on Isolated Tubules—Mice were anesthetized with 50 mg/kg pentobarbital sodium or xylazine/ketamine intraperitoneally. Both kidneys were cooled *in situ* with control bath solution (see below) for 1 min and then removed and cut into thin coronal slices for tubule dissection. CCDs were dissected from the cortex at 10°C in the control solution. *In vitro* microperfusion of single CCD segments, intracellular pH, and transepithelial NH_3 permeability measurements were performed as described previously (13).

Intracellular pH Measurement—The isolated tubule was transferred to the bath chamber on the stage of an inverted microscope (Axiovert 200, Carl Zeiss, Germany) in the control

solution containing (in mM) 138 NaCl, 1.5 CaCl₂, 1.2 MgSO₄, 2 K₂HPO₄, 10 HEPES, 5.5 glucose, 5 alanine, pH 7.40, and then was mounted on concentric pipettes and perfused *in vitro* with Na⁺-free, ammonium-free solution, where *N*-methyl-D-glutamine⁺ (NMDG⁺) replaced Na⁺. All solutions were equilibrated with 100% O₂ passed through a 3 N KOH CO₂ trap. Once the solutions were gassed and the pH checked, they were placed in a reservoir and were continuously bubbled with 100% O₂. The average tubule length exposed to bath fluid was limited to 300–350 μm to prevent motion of the tubule. CCDs or OMCDs were loaded with 5 μM of the fluorescent probe 2',7'-bis(2-carboxyl)-5-(and-6)-carboxyfluorescein (BCECF Invitrogen) for ~20 min at 37 °C in the control bath solution. The loading solution was then washed out by initiation of bath flow, and the tubule was equilibrated with dye-free control bath solution for 5 min. Bath solution was delivered at a rate of 20 ml/min and warmed to 37 °C by a water jacket immediately upstream to the chamber. After this temperature equilibration in control solution, tubules were first transiently acidified by peritubular Na⁺ removal (sodium-free, ammonium-free solution) (10 min duration), replaced by NMDG⁺ to avoid exit of NH₄⁺ by basolateral Na⁺-coupled transport. This maneuver was done in the luminal absence of Na⁺. During the fluorescence recording, perfusion solution was delivered to the perfusion pipette via a chamber under an inert gas (N₂) pressure (around 1 bar) connected through a manual six-way valve. With this system, opening of the valve instantaneously activates flow of solutions. The majority of the fluid delivery to the pipette exits the rear of the pipette system through a drain port at 4 ml/min. This method results in a smooth and complete exchange of the luminal or the peritubular solution in less than 3–4 s (27). After the fluorescence signal stabilization, luminal medium was instantly (at the rate of 4 ml/min in the draining) replaced by a Na⁺-free solution containing 20 mM NH₄Cl (and 118 mM NMDG-Cl) that elicited a rapid intracellular alkalinization, followed by a sharp acidification. The rate of intracellular alkalinization has been associated with the entry of NH₃, whereas the subsequent phase of intracellular acidification in the continued presence of extracellular NH₄Cl reflects mostly NH₄⁺ entry (28). Fluorescence monitoring and calibration were performed with a video imaging system (Visitron Systems, Germany) as described previously (11, 13). For peritubular ammonium pulse, peritubular solution was changed by a 6 mM NH₄Cl solution, pH 7.40. in the presence of 1 mM furosemide and 2.5 mM ouabain in the bath.

Intrinsic Buffering Capacity Determination—The intrinsic buffering capacity (β_i) of CCD cells was determined, as reported previously (29), using a 40 mM NH₄Cl basolateral pulse to acidify the cells. To exclude HCO₃⁻/CO₂ as a buffering component and block Na⁺-dependent pH_i regulatory mechanisms, Na⁺-free, HEPES-buffered solutions were used in the perfusate; the bath contained 1 mM amiloride (to inhibit Na⁺/H⁺ exchangers), and bath and perfusate also contained 100 μM Sch28080 (to block H⁺/K⁺-ATPases) and 200 nM concanamycin A (to block H⁺-ATPases). Addition of 40 mM NH₄Cl to the bath induced an increase following by a decrease in pH_i. The pK_a of ammonia (9.03) was used to calculate the intracellular NH₄⁺ concentration when cell acidification plateaued. β_i was calculated as the ratio of the change in intracel-

lular NH₄⁺ concentration to the change in pH_i. Therefore, we determined the correlation between intracellular pH and β_i, which was -32.7–22.3·pH in wild types, -2.3–8.2·pH in heterozygotes, and 1.4–5.0·pH_i in *Rhcg*^{-/-} mice. We measured cellular buffering power (β_i) in CCDs from all three genotypes of mice.

NH₃ Permeability Measurement—The basic approach used to determine NH₃ permeability involved construction of a transepithelial gradient of NH₃ and measurement of the resulting NH₃ flux from the basolateral to the luminal side as described previously (11, 13, 30). The isolated CCD was transferred to the bath chamber on the stage of an inverted microscope (Axiovision A1, Zeiss, Germany) and mounted on concentric glass pipettes for microperfusion. Bath solution was delivered at a rate of 20 ml/min and warmed to 37 °C by a water jacket immediately upstream of the chamber. The perfusion rate was adjusted by hydrostatic pressure to ~10 nl/min. The tubules were equilibrated for 20–30 min at 37 °C before the beginning of collections. To construct a transepithelial NH₃ gradient, the perfusion (lumen) solution contained (in mM) 139 NaCl, 1 NH₄Cl, 2.5 K₂HPO₄, 2 NaHCO₃, pH 6.4; the bath solution contained (in mM) 117 NaCl, 1 NH₄Cl, 2.5 K₂HPO₄, 23 NaHCO₃, pH 7.4, and in addition, both solutions contained (in mM) 5.5 glucose, 2 CaCl₂, 1.2 MgSO₄ and 10 HEPES. The osmolarity of the solution was 295 ± 5 mosmol/kg H₂O. All solutions were equilibrated with 95% O₂, 5% CO₂. Once the solutions were gassed and the pH checked, they were placed in a reservoir and continuously bubbled with 95% O₂, 5% CO₂. The actual pH of the solutions was monitored several times during the experiments, and the pH of solutions was checked at the end of the experiment to ensure that changes did not occur. Carbonic anhydrase (Sigma) was added to the perfusate solution (1 mg/10 ml of solution). The purpose of carbonic anhydrase was to prevent any pH disequilibrium that might arise from proton secretion or NH₃ transport. Total ammonium concentration was measured in 10–12-nl samples of peritubular, perfused, and collected fluids using an NH₃ diagnostic kit (Sigma) and the flow-through microfluorometer Nanoflow apparatus (World Precision Instruments, UK) (31).

Calculations of Transepithelial NH₃ Permeability—Assuming an absence of osmotic or hydrostatic pressure gradients across the epithelium and therefore an absence of net fluid transport, the passive transepithelial transport of total ammonium (Am) may be described by Equation 1,

$$J_{Am} = P_{NH_3} \times A_S \times \Delta C_{NH_3} \quad (\text{Eq. 1})$$

where P_{NH_3} is diffusive permeability of NH₃ (cm/s), A_S is tubule luminal surface area (cm²), and ΔC_{NH_3} is the transepithelial concentration difference for NH₃ (mM). To calculate the permeability to NH₃, Equation 1 is rearranged as Equation 2,

$$P_{NH_3} = J_{Am} / (A_S \times \Delta C_{NH_3}) \quad (\text{Eq. 2})$$

The net rate of transport J_{Am} is calculated as shown in Equation 3,

$$J_{Am} = ([Am]_i - [Am]_o) \times V/L \quad (\text{Eq. 3})$$

Incomplete dRTA in *Rhcg*-targeted Mice

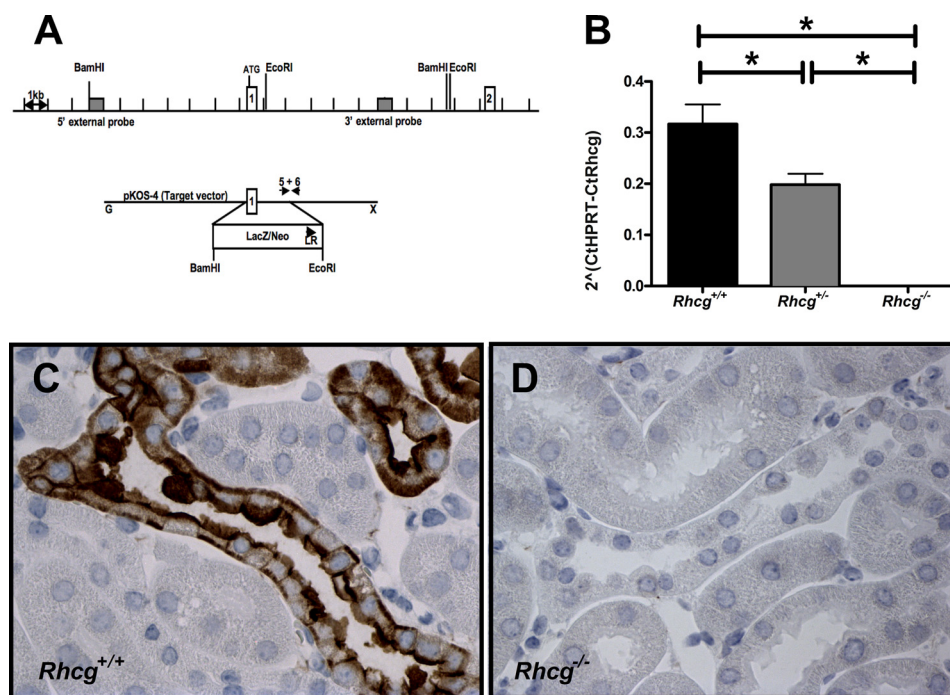


FIGURE 1. *Rhcg* gene targeting and deletion. *A*, *Rhcg* gene knock-out was achieved by replacement of exon 1 by a LacZ/neomycin cassette (Texas Institute of Genomic Medicine, Houston, TX). *B*, RT-quantitative PCR with primers placed in exon 1 of *Rhcg* demonstrated lower mRNA in kidneys from *Rhcg*^{+/-} mice and absence of a detectable PCR product in kidneys from *Rhcg*^{-/-} mice (*n* = 5 mice). *C* and *D*, *Rhcg* immunodetection in kidney sections from wild type (*C*) and *Rhcg*^{-/-} (*D*) mice. * indicates significantly different *p* < 0.05.

where $[Am]_i$ is the concentration of total ammonium in the perfusate; $[Am]_o$ is the concentration of total ammonium in the collected fluid; V is the collection rate (nl/min), as measured in precalibrated constriction pipettes, and L is the perfused tubule length (mm). A_s may be calculated as $L\pi d$, where d (mm) is the inner tubule diameter. The total ammonium concentration ($[Am]$) is equal to the sum of the concentrations of the two species NH_3 and NH_4^+ and is the quantity actually measured by the microfluorimetric assay. The equilibrium between the two species is defined by the Henderson-Hasselbalch Equation 4,

$$pH = pK_a + \log\left(\frac{[NH_3]}{[NH_4^+]}\right) \quad (\text{Eq. 4})$$

The pK_a equals 9.03 at physiological pH and temperature. Knowing the values for pH and $[Am]$, the values for $[NH_3]$ and $[NH_4^+]$ may be determined simultaneously.

Statistics—Data are expressed as means \pm S.E. Statistical comparisons were tested by analysis of variance and Student's *t* test using the Graphpad Prism software (GraphPad). *p* values < 0.05 were considered as statistically significant.

RESULTS

Deletion of *Rhcg* in Mice—Mice lacking *Rhcg* were generated using gene trap technology in a mixed genetic background (129SvEvBrd, C57/BL6) (Fig. 1*A*) and were purchased from the Texas Institute of Genomic Medicine (32). *Rhcg* mRNA was undetectable in renal tissue from *Rhcg* knock-out (*Rhcg*^{-/-}) mice and reduced by ~50% in heterozygous mice (*Rhcg*^{+/-}) mice (Fig. 1*B*). RhCG protein was completely absent from the kidney of *Rhcg*^{-/-} mice as confirmed by immunohistochemistry (Fig. 1*C*).

Heterozygous Mice Develop Metabolic Acidosis While on Long Term Acid Load—We first assessed acid-base status under basal conditions and during an acid load in *Rhcg* litter-

mates. Throughout the study, food intake was similar in all three genotypes. At base line, no difference in acid-base and electrolyte levels was observed (Tables 1 and 2).

The effects of both acute (2 days) and chronic (7 days) HCl load were tested (Tables 1–3 and Fig. 2). On the 2nd day of the HCl load, blood pH and HCO_3^- concentration were decreased in all genotypes, as compared with base line (Table 1, and Fig. 2, *D* and *E*). Blood pH and HCO_3^- concentrations were significantly lower in *Rhcg*^{-/-} mice but similar in *Rhcg*^{+/-} and *Rhcg*^{+/+} mice. Urinary ammonium excretion rate increased significantly on the 1st day of acid loading in *Rhcg*^{+/+} and *Rhcg*^{+/-} mice but much less in *Rhcg*^{-/-} mice (Tables 2 and 3 and Fig. 2*A*). Urinary pH decreased in *Rhcg*^{+/+} and *Rhcg*^{+/-} mice as compared with base-line values (Table 2 and Fig. 2*B*) but to a lesser extent in *Rhcg*^{-/-} mice. Urinary titratable acid excretion was unaltered in all three genotypes during the acute acid load. Long term HCl loading resulted in the death of most *Rhcg*^{-/-} mice, which poorly excreted ammonium and exhibited a very severe metabolic acidosis. These animals showed a higher loss of body weight after the acute HCl load presumably due to dehydration (Table 3).

In contrast to the *Rhcg*^{+/+} mice, which adapted and nearly normalized their blood pH and HCO_3^- concentration, *Rhcg*^{+/-} remained acidotic at day 7 of the HCl load, even though both genotypes maintained a high NH_4^+ excretion. At the end of the chronic acid load, *Rhcg*^{+/-} mice showed less increase in their titratable acid excretion and had a more alkaline urine pH (Tables 1 and 2 and Fig. 2, *B* and *C*). Thus, both *Rhcg*^{-/-} and *Rhcg*^{+/-} exhibited renal acid handling defects.

Absence of RhCG Abolishes Medullary Ammonium Accumulation—To assess the cortico-papillary gradient of NH_3/NH_4^+ in kidneys from *Rhcg* mice, we measured ammonium content in

TABLE 1
Blood values in *Rhcg* littermates mice under normal diet and during an acid load

	Basal status			2 days HCl			7 days HCl		
	<i>Rhcg</i> ^{+/+} (n = 10)	<i>Rhcg</i> ^{+/-} (n = 16)	<i>Rhcg</i> ^{-/-} (n = 9)	<i>Rhcg</i> ^{+/+} (n = 10)	<i>Rhcg</i> ^{+/-} (n = 10)	<i>Rhcg</i> ^{-/-} (n = 9)	<i>Rhcg</i> ^{+/+} (n = 12)	<i>Rhcg</i> ^{+/-} (n = 21)	<i>Rhcg</i> ^{-/-} (n = 2)
pH	7.38 ± 0.02	7.38 ± 0.02	7.28 ± 0.04 ^a	7.17 ± 0.02 ^a	7.17 ± 0.02 ^a	7.07 ± 0.02 ^{a,b}	7.24 ± 0.03 ^a	7.17 ± 0.02 ^{a,b}	6.88 ± 0.07
pCO ₂ (mm Hg)	34.0 ± 1.3	37.2 ± 0.9	38.8 ± 1.4 ^a	41.2 ± 2.0 ^a	39.4 ± 0.7	37.8 ± 0.9	42.0 ± 1.4 ^a	40.0 ± 0.8	44.6 ± 1.6
HCO ₃ ⁻ (mM)	19.0 ± 1.1	22.4 ± 1.0	18.3 ± 2.1	14.3 ± 0.6 ^a	13.8 ± 0.5 ^a	11.1 ± 0.6 ^{a,b}	18.6 ± 1.3	13.9 ± 0.6 ^{a,b}	7.9 ± 1.05
pO ₂	74.7 ± 9.7	52.3 ± 3.4	63.6 ± 6.3	60.1 ± 2.3	59.4 ± 1.4	65.7 ± 4.1	57.1 ± 3.0	63.1 ± 3.4	82.3 ± 4.6
Na ⁺ (mM)	143.9 ± 1.5	145.4 ± 0.9	148.0 ± 0.4	150.1 ± 1.0	145.8 ± 0.8	150.4 ± 0.9	148.3 ± 0.6	149.1 ± 0.5	148.5 ± 1.5
Cl ⁻ (mM)	117.5 ± 1.9	112.1 ± 1.7	111.7 ± 1.5	123.7 ± 1.0 ^a	119.7 ± 1.0 ^a	126.4 ± 0.9 ^a	118.9 ± 0.9	122.6 ± 0.7 ^{a,b}	134.0 ± 0.0
Ionized Ca ²⁺ (mM)	1.23 ± 0.02	1.25 ± 0.01	1.29 ± 0.03	1.41 ± 0.03 ^a	1.35 ± 0.01 ^a	1.42 ± 0.02 ^a	1.34 ± 0.01 ^a	1.37 ± 0.01 ^{a,b}	1.01 ± 1.9
Glucose (mM)	10.6 ± 0.7	10.9 ± 0.5	10.8 ± 0.8	7.8 ± 0.4 ^a	9.0 ± 0.3 ^b	6.5 ± 0.4 ^{a,b}	9.6 ± 0.4	8.8 ± 0.3 ^a	ND ^c
Hb (g/dl)	15.0 ± 1.1	15.7 ± 0.3	16.3 ± 0.5	16.3 ± 0.4	15.5 ± 0.3	17.5 ± 0.3 ^{a,b}	15.2 ± 0.5	14.9 ± 0.4	17.4 ± 1.0

^a *p* < 0.05 versus base-line period in same genotype is shown.
^b *p* < 0.05 versus *Rhcg*^{+/+} mice during the same period is shown.
^c ND, not determined.

TABLE 2
Weight, food intake, and urinary values in *Rhcg* littermate mice under a normal diet and a 2-day HCl load

TA means titratable acid; NA means net acid; UNH₄ means urinary ammonium; UCr means urinary creatinine; UTa means urinary titratable acids; UP_i means urinary inorganic phosphate; Uurea means urinary urea; UNa means urinary Na⁺; UCl means urinary Cl⁻; and UK means urinary K⁺.

	Basal status			2 days of HCl		
	<i>Rhcg</i> ^{+/+} (n = 14)	<i>Rhcg</i> ^{+/-} (n = 13)	<i>Rhcg</i> ^{-/-} (n = 13)	<i>Rhcg</i> ^{+/+} (n = 14)	<i>Rhcg</i> ^{+/-} (n = 13)	<i>Rhcg</i> ^{-/-} (n = 13)
Weight (g)	26.4 ± 0.6	28.7 ± 1.2	27.6 ± 1.0	24.9 ± 0.5	26.6 ± 0.8	25.0 ± 1.1
Weight lose in % of body weight under basal status	ND ^a	ND	ND	8.3 ± 0.4	11.4 ± 1.3	15.0 ± 1.0 ^b
Food intake (g/24 h/body weight)	0.31 ± 0.06	0.26 ± 0.02	0.26 ± 0.02	0.24 ± 0.01	0.21 ± 0.01	0.21 ± 0.02
Urine values						
Volume (ml/24 h)	1.9 ± 0.2	2.0 ± 0.1	1.9 ± 0.1	2.5 ± 0.3	2.1 ± 0.2	2.1 ± 0.4 ^c
Creatinine excretion (μmol/24 h)	7.6 ± 0.3	6.2 ± 0.6	7.8 ± 0.4	7.5 ± 0.7	5.6 ± 1.4	8.3 ± 2.3
Urinary pH	6.13 ± 0.04	6.18 ± 0.06	6.03 ± 0.06	5.47 ± 0.05 ^c	5.44 ± 0.02 ^c	5.68 ± 0.06 ^{b,c}
UNH ₄ /UCr (mEq/mmol)	4.6 ± 1.0	5.1 ± 0.7	4.1 ± 1.0	37.8 ± 4.1 ^c	43.8 ± 6.0 ^c	11.1 ± 1.5 ^{b,c}
UTA/UCr (mEq/mmol)	15.4 ± 1.2	14.4 ± 1.0	13.6 ± 1.1	20.9 ± 2.5	15.9 ± 3.2	14.5 ± 1.9
UP _i /UCr (mEq/mmol)	16.1 ± 1.7	20.3 ± 1.0	17.7 ± 1.4	9.3 ± 1.5	10.7 ± 1.7	8.2 ± 1.6
Uurea/UCr (mg/mmol)	266.3 ± 14.8	279.3 ± 14.8	280.8 ± 15.0	229.2 ± 17.1	255.1 ± 24.01	146.8 ± 15.7 ^{b,c}
UNa/UCr (mEq/mmol)	20.0 ± 1.4	19.4 ± 0.8	17.7 ± 1.3	58.7 ± 4.9 ^c	60.9 ± 9.0 ^c	25.6 ± 2.9 ^{b,c}
UNa/UCr (mEq/mmol)	16.8 ± 2.0	10.0 ± 2.0	15.5 ± 2.0	15.4 ± 1.6	15.8 ± 3.6	9.7 ± 1.7
UCl/UCr (mEq/mmol)	32.8 ± 2.0	30.6 ± 1.7	32.6 ± 2.3	133.0 ± 14.4 ^c	132.3 ± 19.8 ^c	40.5 ± 9.2 ^{b,c}
UK/UCr (mEq/mmol)	60.1 ± 3.9	60.2 ± 4.6	63.1 ± 4.9	53.9 ± 4.3	56.3 ± 7.3	27.7 ± 3.2

^a ND, not determined.
^b *p* < 0.05 versus *Rhcg*^{+/+} mice during the same period is shown.
^c *p* < 0.05 versus base-line period in same genotype is shown.

TABLE 3
Weight, food intake, and urinary values in 3-month-old *Rhcg*^{+/+} and *Rhcg*^{+/-} littermates during 6 or 7 days of HCl load

TA means titratable acid; NA means net acid; UNH₄ means urinary ammonium; UCr means urinary creatinine; UTa means urinary titratable acids; UP_i means urinary inorganic phosphate; Uurea means urinary urea; UNa means urinary Na⁺; UCl means urinary Cl⁻; and UK means urinary K⁺.

	6 days of HCl			7 days of HCl	
	<i>Rhcg</i> ^{+/+} (n = 8)	<i>Rhcg</i> ^{+/-} (n = 10)	<i>Rhcg</i> ^{-/-} (n = 2)	<i>Rhcg</i> ^{+/+} (n = 8)	<i>Rhcg</i> ^{+/-} (n = 10)
Weight (g)	ND ^a	ND	19.6–22.4	25.1 ± 1.2	23.3 ± 0.8 ^b
Weight lose in % of body weight under basal status	ND	ND	ND	10.0 ± 1.1 (n = 5)	14.8 ± 2.1 (n = 5)
Food intake (g/24 h/body weight)	ND	ND	0.31–0.44	0.37 ± 0.03	0.39 ± 0.02
Urine values					
Volume (ml/24 h)	3.8 ± 0.8 ^b	4.4 ± 0.8 ^b	2.5–2.6	3.1 ± 0.2 ^b	3.9 ± 0.1 ^b
^a Creatinine excretion (μmol/24 h)	8.5 ± 2.0	7.2 ± 1.8	3.8–4.3	6.6 ± 0.3	7.9 ± 1.4
^a Urinary pH	5.39 ± 0.13 ^b	5.59 ± 0.07 ^b	5.20–5.52	5.57 ± 0.02 ^b	5.73 ± 0.05 ^{b,c}
^a UNH ₄ /UCr (mEq/mmol)	153.9 ± 31.1 ^b	173.1 ± 20.6 ^b	17.3–36.3	147.4 ± 26.3 ^b	171.8 ± 22.3 ^b
^a UTA/UCr (mEq/mmol)	25.4 ± 2.6 ^b	17.9 ± 2.5	28.6–36.2	26.3 ± 0.6 ^b	16.6 ± 0.7 ^c
^a UP _i /UCr (mEq/mmol)	ND	ND	ND	9.8 ± 3.7	25.0 ± 8.8
^a UNa/UCr (mEq/mmol)	131.2 ± 6.3 ^b	128.5 ± 16.4 ^b	68.9–53.4	126.8 ± 9.8	118.3 ± 15.0
^a Uurea/UCr (mg/mmol)	205.2 ± 11.2 ^b	220.3 ± 9.9 ^b	186.4–230.1	208.9 ± 6.3 ^b	220.6 ± 5.5 ^b
^a UNa/UCr (mEq/mmol)	36.9 ± 3.8 ^b	32.9 ± 2.8 ^b	67.4–70.9	43.0 ± 3.0 ^b	38.4 ± 4.0 ^b
^a UCl/UCr (mEq/mmol)	242.6 ± 11.2 ^b	253.6 ± 11.4 ^b	135.1–173.1	269.5 ± 12.0 ^b	263.5 ± 14.9 ^b
^a UK/UCr (mEq/mmol)	77.6 ± 4.2	79.7 ± 4.1	19.6–22.4	92.2 ± 2.0	85.2 ± 9.9

^a ND means not determined.
^b *p* < 0.05 versus base-line period in the same genotype.
^c *p* < 0.05 versus *Rhcg*^{+/+} mice during the same period.

the cortex and outer and inner medulla after 4 days of HCl treatment. There was no difference between *Rhcg*^{+/+} and *Rhcg*^{+/-} mice. However, the inner medulla ammonium content was strongly reduced to 39% in *Rhcg*^{-/-} mice (Fig. 3). Thus, the absence of *Rhcg* impairs the ability to concentrate ammonium in the interstitium of the inner medulla.

RhCG Is Located at the Apical and Basolateral Sides of Cells Along the Distal Nephron—RhCG has been localized to most cells of the CD, including type A intercalated cells as well as principal cells (9, 17). However, the subcellular localization of RhCG has remained controversial because some groups reported both apical and basolateral staining (10, 17), whereas

Incomplete dRTA in *Rhcg*-targeted Mice

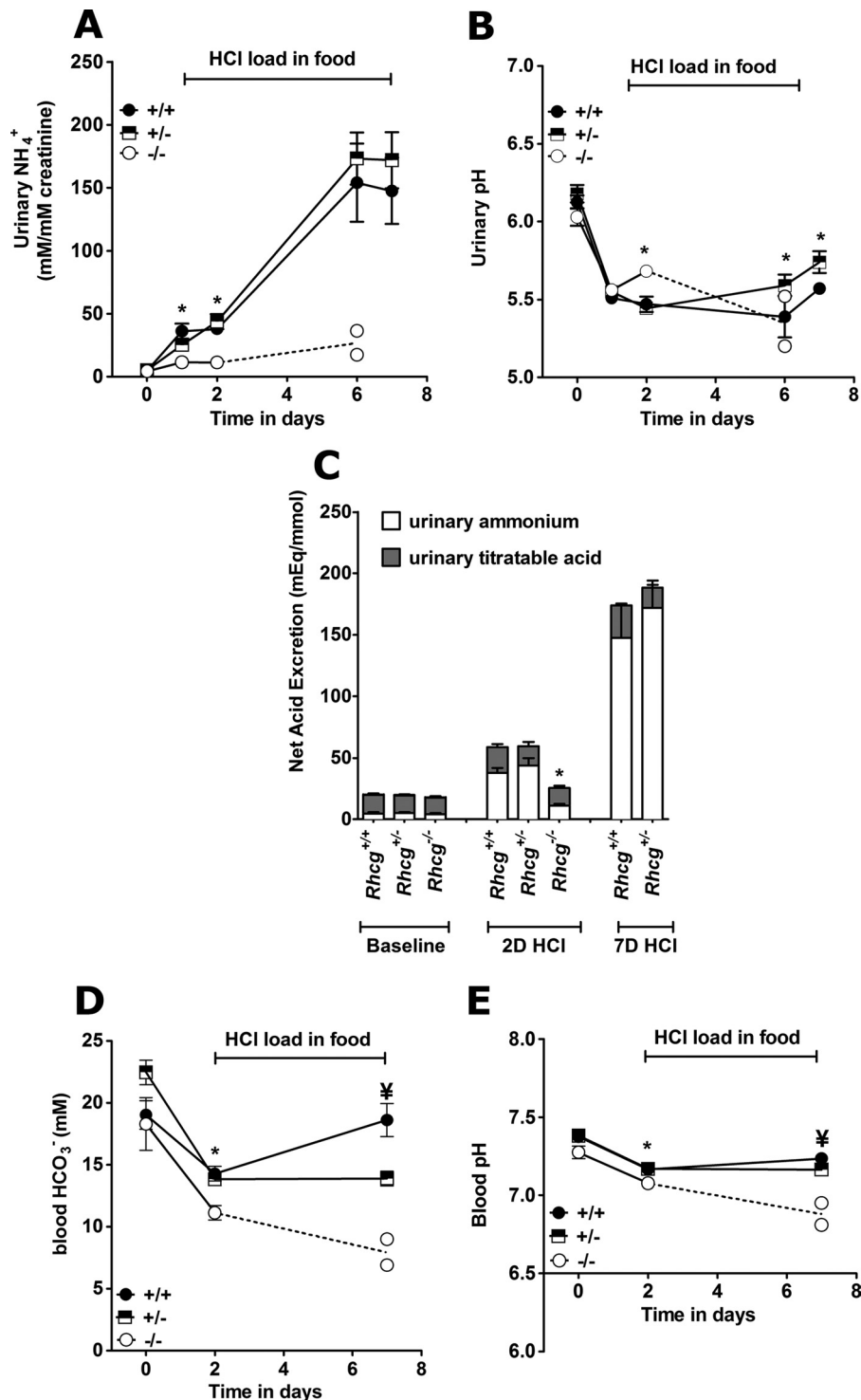


FIGURE 2. Incomplete dRTA in *Rhcg*^{+/-} and *Rhcg*^{-/-} mice. Mice were observed in metabolic cages under basal conditions and during an acid load for up to 7 days with HCl added to the diet ($n = 5-10$ per genotype). *Rhcg*^{-/-} could only be observed for 6 days during the HCl-containing diet because most animals had to be terminated earlier. *A*, urinary ammonium excretion in 24-h urine collections normalized for urinary creatinine. *B*, urinary pH in 24-h urine collections. *C*, urinary net acid excretion (total bars) calculated from urinary ammonium (open bars) plus titratable acid (gray bars). Urinary bicarbonate levels were measured and negligible. *D*, blood bicarbonate concentrations. *E*, blood pH values. *, $p < 0.05$ for *Rhcg*^{-/-} versus *Rhcg*^{+/+}. †, $p < 0.05$ for *Rhcg*^{+/-} versus *Rhcg*^{+/+}.

others detected only apical staining for RhCG (9) based on different immunohistochemical methods. We confirmed a strong labeling of both apical and basolateral poles of CD cells in mouse kidneys (Fig. 4 and Table 4). This staining was absent from *Rhcg*^{-/-} kidneys demonstrating its specificity. In the kidney cortex, RhCG was localized in the distal convoluted tubule,

connecting tubule, and CCD (Fig. 4A). In the distal convoluted tubule cells, RhCG was mainly present at the apical side (Fig. 4A). In the connecting tubule, CCD and OMCD, both intercalated and principal cells, were stained. Principal cells and some intercalated cells exhibited RhCG staining at both the apical and basolateral sides (Fig. 4, A-C). However, in some cells

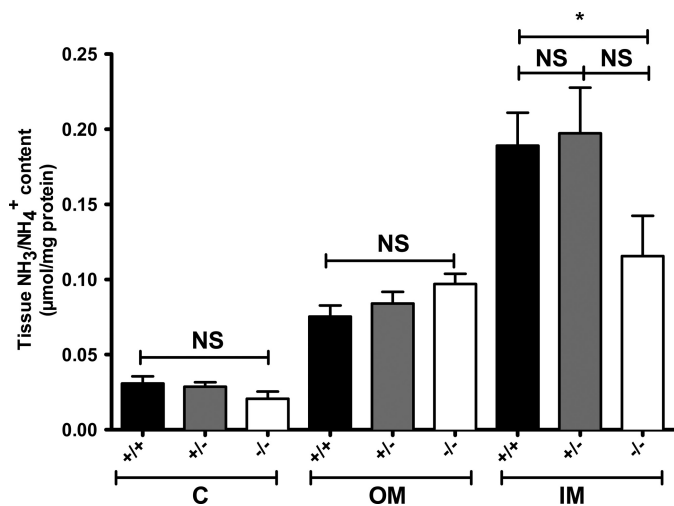


FIGURE 3. Medullary ammonium accumulation is altered in *Rhcg*^{-/-} mice. Kidneys from all three genotypes were dissected after 4 days of HCl load. Cortex (C), outer medulla (OM), and inner medulla (IM) were separated, and tissue ammonium content was measured. In wild type and heterozygous mice, a gradient in renal tissue ammonia content from cortex to inner medulla was observed. In *Rhcg*^{-/-} mice, the ammonia content increased from cortex to outer medulla, but ammonium content was lower in the inner medulla than in mice from the other two genotypes. ($n = 5\text{--}8$ mice/genotype), * statistically different from *Rhcg*^{+/+} mice ($p < 0.05$). NS, not significant.

RhCG was strictly localized at the apical pole (see arrowheads in Fig. 4, A, B, and D). These cells have been previously identified as non-A/non-B type intercalated cells (33, 34). Finally, in the inner medulla, only strong apical and faint basolateral staining were found in intercalated cells (Fig. 4 and Table 4). Immunogold electron microscopy demonstrated RhCG associated with the apical membrane as well as the basolateral interdigitations of segment specific and intercalated cells (Fig. 4, E and F). No specific immunogold labeling was found in kidneys from *Rhcg*^{-/-} mice (data not shown). Thus, RhCG protein is expressed on both apical and basolateral membranes in mouse segment-specific principal and intercalated CD cells.

Total and Apical Membrane Permeabilities for NH₃ Are Reduced in CDs from *Rhcg*^{+/-} Mice—We assessed total transepithelial permeability for NH₃ in *in vitro* microperfused cortical CDs from *Rhcg* mice after a 2-day HCl diet, a condition causing a strong difference in urinary ammonium excretion between *Rhcg*^{+/+} and *Rhcg*^{-/-} mice. Imposing a bath-to-lumen NH₃ gradient in the nominal absence of an NH₄⁺ gradient generated a measurable NH₃ secretory flux, which was significantly lower in CCDs from *Rhcg*^{+/-} and *Rhcg*^{-/-} mice versus *Rhcg*^{+/+} mice. These differences were due to a decrease in transepithelial permeability to NH₃ by 54 and 83%, respectively (Table 5 and Fig. 5). Thus, one *Rhcg* allele was not sufficient to sustain normal transepithelial permeability to NH₃ in the mouse collecting duct.

Next, we tested whether the apical permeability to NH₃ was affected in CDs from *Rhcg*^{+/-} mice. Therefore, we measured the effects of an inwardly directed gradient on pHi on CCDs isolated from *Rhcg*^{+/+} and *Rhcg*^{+/-} mice (13). Fig. 6A depicts the typical time course of pHi changes when NH₃/NH₄⁺ was added to the lumen tubule. The initial rate of cellular alkalization is proportional to the rate of apical NH₃ entry as described previously (13, 35, 36). To directly compare transport

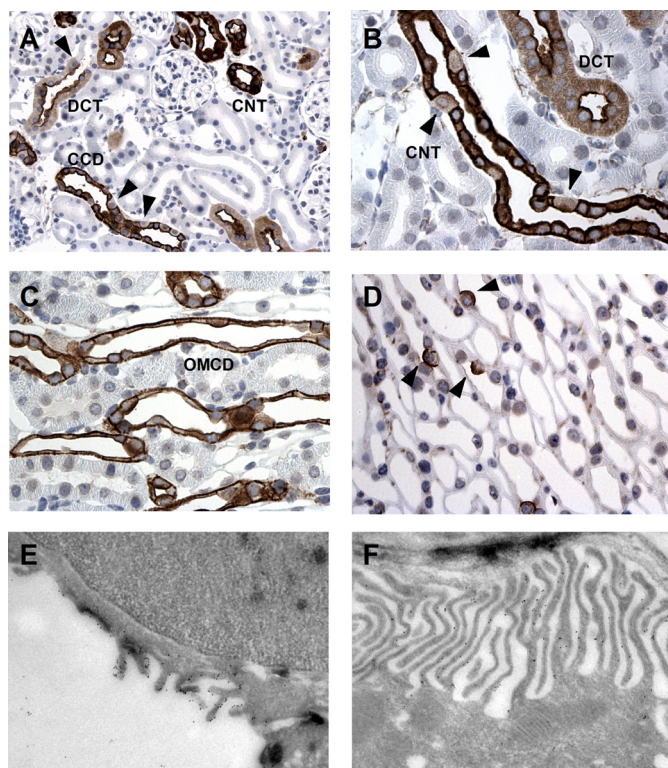


FIGURE 4. *Rhcg* immunodetection in mouse kidney and immunogold electron microscopic localization of *Rhcg* in CCD. A and B, *Rhcg* protein immunodetection in mouse kidney cortex. *Rhcg*-related staining was detected in the distal convoluted tubule (DCT) starting immediately at the transition from the thick ascending limb (TAL) to the distal convoluted tubule (arrowhead), in the connecting tubule (CNT) and CCD. Most but not all cells are stained. *Rhcg* staining is observed in most cells at the apical and basolateral sides, but in some cells (arrowheads) only an apical signal is detected. C, *Rhcg* immunodetection in outer medulla. *Rhcg* is strictly expressed in collecting ducts at both sides of intercalated and segment-specific cells. D, in the inner medulla, *Rhcg* is expressed only in intercalated cells. E and F, *Rhcg* was detected both at the apical membrane (E) and at the invaginations of the basolateral membrane (F) of segment-specific cells in the cortical collecting duct by gold immunoelectron microscopy.

rates, we measured intracellular buffering power and calculated the amount of H⁺ used to titrate NH₃ transported across the membrane. Fig. 6B depicts the calculated rate of NH₃ transported into CDs from *Rhcg*^{+/+} and *Rhcg*^{+/-} mice, which was drastically reduced in *Rhcg*^{+/-} tissue.

Basolateral RhCG Accounts for Peritubular Membrane Permeability to NH₃—Because RhCG is expressed at both sides of at least a subset of CD cells (Fig. 4 and Table 4), we next tested the effect of *Rhcg* disruption on NH₃ transport across the basolateral membranes of CCD cells. Several transport pathways for NH₄⁺ have been proposed at the basolateral side of CD cells, including the Na⁺-K⁺-2Cl⁻ cotransporter NKCC1 and the Na/K-ATPase where NH₄⁺ would substitute for K⁺ (37, 38). Therefore, we performed experiments in the nominal absence of sodium to block the activity of both transport pathways.

Peritubular NH₃/NH₄⁺ prepulses were performed on cortical CDs from *Rhcg*^{+/+}, *Rhcg*^{+/-}, and *Rhcg*^{-/-} mice submitted to HCl loading for 2 days. As summarized in Fig. 7, when NH₃/NH₄⁺ (6 mM) was applied to the basolateral side, the calculated rate of NH₃ transport into CD cells was unchanged in *Rhcg*^{+/-} tissue but strongly reduced in *Rhcg*^{-/-} tissue. Thus, RhCG sustains both apical and basolateral transport of NH₃ in CD cells, in agreement

Incomplete dRTA in *Rhcg*-targeted Mice

TABLE 4

Summary of RhCG localization along the mouse nephron

CNT is connecting tubule; DCT is distal convoluted tubule.

	Tubule type	Cell type	Localization	Staining intensity
Cortex	DCT		Apical	High
			Basolateral	Weak
	CNT	Principal cells	Plasma membrane	High
Outer medulla	CCD	Intercalated cells	Plasma membrane/apical	High
		Principal cells	Plasma membrane	High
	OMCD	Intercalated cells	Plasma membrane/apical	High
		Principal cells	Plasma membrane/apical	High
Inner medulla	IMCD	Principal cells	No staining	
		Intercalated cells	Plasma membrane/apical	Weak/high

TABLE 5

CCD *in vitro* microperfusion data from *Rhcg*^{+/+}, *Rhcg*^{+/-}, and *Rhcg*^{-/-} mice

Values are mean ± S.E.; *n* means no. of mice.

	<i>Rhcg</i> ^{+/+} (<i>n</i> = 7)	<i>Rhcg</i> ^{+/-} (<i>n</i> = 9)	<i>Rhcg</i> ^{-/-} (<i>n</i> = 5)
Tubule length, mm	0.38 ± 0.04	0.36 ± 0.05	0.034 ± 0.08
Tubule diameter, μm	54.98 ± 4.55	47.92 ± 4.24	44.31 ± 8.88
Collection rate, nl·mm ⁻¹ ·min ⁻¹	4.61 ± 0.22	4.37 ± 0.29	3.96 ± 0.42
Perfusate pH	6.44 ± 0.04	6.37 ± 0.04	6.50 ± 0.04
Bath pH	7.42 ± 0.03	7.37 ± 0.03	7.38 ± 0.03
Total ammonia perfusate, mM	1.41 ± 0.08	1.40 ± 0.08	1.42 ± 0.13
[NH ₃] perfusate, μM	3.74 ± 0.37	3.30 ± 0.32	4.16 ± 0.25
Total ammonia bath, mM	1.41 ± 0.08	1.40 ± 0.08	1.42 ± 0.13
[NH ₃] bath, μM	34.38 ± 3.26	32.57 ± 3.72	31.39 ± 3.71
Total ammonia collected, mM	3.88 ± 0.42	2.47 ± 0.36	1.48 ± 0.35
[NH ₃] collected, μM	10.37 ± 1.45	5.90 ± 1.24 ^a	4.25 ± 0.93 ^a
Total ammonia flux, pmol·mm ⁻¹ ·min ⁻¹	32.98 ± 3.32 ^a	17.84 ± 4.56 ^a	2.51 ± 3.51 ^a
NH ₃ permeability, mm/s	0.13 ± 0.02	0.08 ± 0.02 ^a	0.02 ± 0.02 ^a

^a *p* < 0.05 versus control mice.

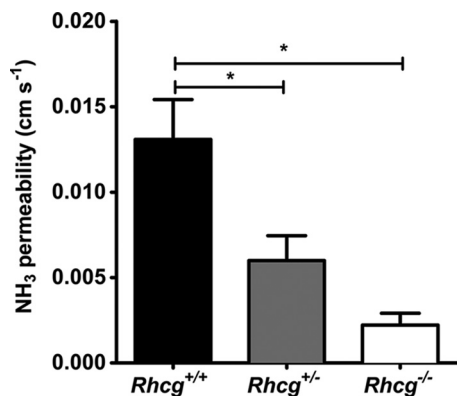


FIGURE 5. Transepithelial NH₃ permeability is reduced in the cortical collecting duct from *Rhcg*^{+/-} and *Rhcg*^{-/-} mice. Transepithelial permeability to NH₃ was assessed in *in vitro* isolated and microperfused cortical collecting ducts from mice kept for 2 days on an HCl diet by imposing a bath-to-lumen NH₃ gradient (see under “Experimental Procedures”) (*, *p* < 0.05).

with structural data and reconstituted RhCG suggesting that the protein forms a NH₃-permeable channel (39, 40).

Compensatory Adaptations to the Loss of *Rhcg*—We finally examined whether *Rhcg* deletion affects mechanisms involved in renal ammoniogenesis and ammonium excretion. Surprisingly, immunoblots of whole kidney extracts from mice subjected to a 2-day HCl load revealed no differences in the expression of PEPCK expression (Fig. 8A). In contrast, the expression of the PDG, mediating the initial step of ammoniogenesis was decreased in *Rhcg*^{+/-} kidneys as compared with both *Rhcg*^{+/+} and *Rhcg*^{-/-} kidneys (Fig. 8B). The abundance of the Na⁺/H⁺ exchanger NHE3, involved in NH₄⁺ secretion into the proximal tubule lumen, was unchanged (Fig. 8C). Moreover, the expression of the Na⁺-K⁺-2Cl⁻ cotransporter NKCC2, the main apical NH₄⁺

transporter in the thick ascending limb, was highly down-regulated in kidneys from *Rhcg*^{+/-} and *Rhcg*^{-/-} mice (Fig. 8D).

DISCUSSION

Renal ammonium excretion is critical for acid-base homeostasis and is achieved by a complex process involving various nephron segments (2, 5, 6). A critical role for the Rhesus protein RhCG was demonstrated in tissue-specific and complete knock-out mouse models (13–15). However, metabolic effects of *Rhcg* haploinsufficiency, the role of RhCG in basolateral NH₃ transport in CD cells, and the response of other pathways critical for renal ammoniogenesis and ammonium transport have remained unknown. Based on a novel *Rhcg* mouse model, we show that *Rhcg* haploinsufficiency causes incomplete metabolic acidosis in mice. Next, RhCG contributes to peritubular NH₃ uptake giving functional evidence to the basolateral localization of RhCG in CD cells.

***Rhcg*^{-/-} Mice Develop a Severe Incomplete Renal Tubular Acidosis**—*Rhcg*^{-/-} develop incomplete dRTA as evident from the inability to respond to an acute oral acid load. They showed severe hyperchloremic metabolic acidosis and did not increase urinary ammonium excretion resulting in low net acid excretion. Moreover, these animals had a drastic reduction in their blood HCO₃⁻ concentration and pH. *Rhcg*^{-/-} mice developed severe dehydration as indicated by high blood hemoglobin and weight loss (Tables 2 and 4). These phenotypes are more pronounced than in mice with partial deletion of *Rhcg* (14, 15).

***Rhcg* Haploinsufficiency Leads to Metabolic Acidosis**—Similarly, *Rhcg*^{+/-} mice develop also an incomplete dRTA. However, these mice initially responded to the acid load by increasing urinary ammonium excretion to the same extent as

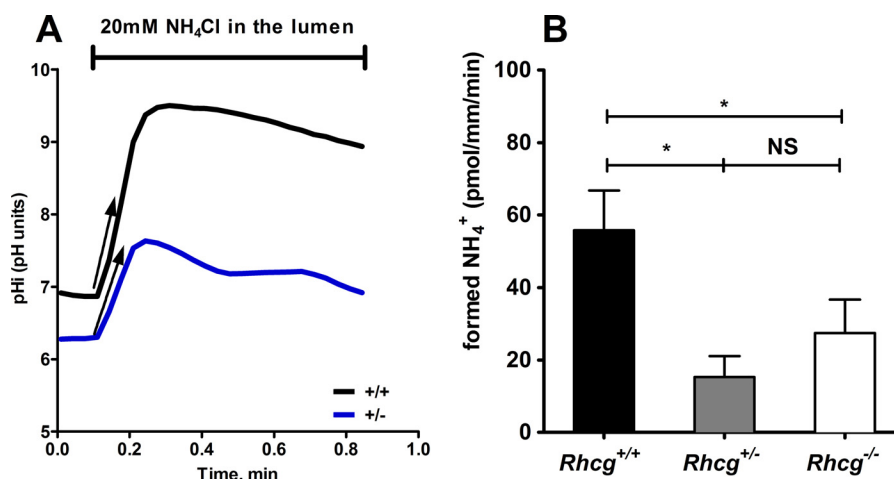


FIGURE 6. RhCG is required for apical NH₃ permeability of cortical collecting duct cells. Cortical collecting ducts were isolated from kidneys of *Rhcg*^{+/+}, *Rhcg*^{+/-}, and *Rhcg*^{-/-} mice after 2 days of HCl loading, and intracellular pH was monitored with BCECF. 20 mM NH₄Cl was applied with the luminal perfusate. **A**, pH_i recording from CCD exposed to a luminal NH₄Cl pulse in *Rhcg*^{+/+} and *Rhcg*^{+/-} CCD. Exposure to NH₄Cl caused a rapid alkalization corresponding to NH₃ entry into cells. The initial slopes ($\Delta\text{pH}_i/\Delta t$) of the alkalization phase were measured, and the amount of NH₃ titrated into NH₄⁺ was finally calculated based on intracellular buffering power. **B**, bar graph summarizing the amount of titrated NH₃ during luminal NH₄Cl pulses ($n = 8-12$ tubules/genotype). *, $p < 0.05$; NS, not significant.

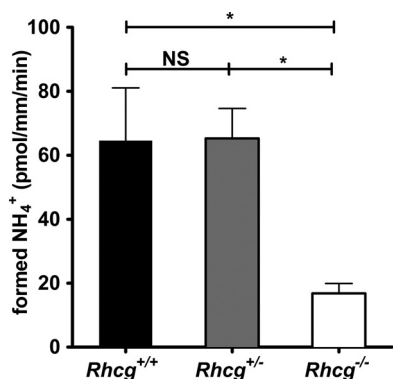


FIGURE 7. Basolateral NH₃ permeability of cortical collecting duct cells. Cortical collecting ducts were isolated from kidneys of *Rhcg*^{+/+}, *Rhcg*^{+/-}, and *Rhcg*^{-/-} mice after 2 days of HCl loading, and intracellular pH was monitored with BCECF. After an equilibrium phase, 6 mM NH₄Cl was applied to the bath. Exposure to NH₄Cl caused a rapid alkalization corresponding to NH₃ entry into cells. The initial slopes ($\Delta\text{pH}_i/\Delta t$) of the alkalization phase were measured, and the amount of NH₃ titrated into NH₄⁺ was finally calculated based on intracellular buffering power. The bar graph summarizes the amount of titrated NH₃ (alkalinization phase) during basolateral NH₄Cl pulses ($n = 5-7$ tubules/genotype). *, $p < 0.05$; NS, not significant.

Rhcg^{+/+} mice. Later, they did not fully adapt to chronic acid loading and remained acidotic after 7 days of HCl loading, being unable to correct blood HCO₃⁻ concentration and excreting more alkaline urine, whereas total net acid excretion was comparable with *Rhcg*^{+/+} animals. The incomplete chronic metabolic acidosis in *Rhcg*^{+/-} mice is at least in part due to the inability to maximally acidify urine and to excrete adequate amounts of acid in the form of titratable acidity. The metabolic phenotype of *Rhcg*^{+/-} mice was further supported by functional studies on microperfused CCDs. Transepithelial permeability to NH₃ was reduced in CCDs from *Rhcg*^{-/-} and *Rhcg*^{+/-} mice. The reduction in NH₃ permeability in CCDs from *Rhcg*^{+/-} mice was less than in *Rhcg*^{-/-} mice, suggesting that a 50% reduction in net NH₃ permeability in CCDs is still sufficient to support high ammonium excretion but is not enough to correct metabolic acidosis. Of note, medullary accumulation of NH₃/NH₄⁺ appeared to be intact. Together, these results repre-

sent the first evidence that loss of a single *Rhcg* allele can lead to chronic hyperchloremic metabolic acidosis.

Renal Adaptation to *Rhcg* Invalidation—We further examined compensatory mechanisms in *Rhcg*^{+/-} and *Rhcg*^{-/-} mice. The generation of the cortico-papillary gradient of ammonium is required for the subsequent uptake of NH₃ and NH₄⁺ by intercalated cells and the secretion of NH₃ into urine. Surprisingly, *Rhcg*^{-/-} mice had low tissue ammonium content in the inner medulla after 4 days of acid loading. This result suggests that the absence of RhCG affects the ability of the medulla to generate or maintain a high interstitium ammonium content. Because the key enzymes of proximal tubular ammoniogenesis, PEPCK and PDG, were normally expressed in *Rhcg*^{-/-} kidney tissue, mice most likely form adequate amounts of ammonium. In *Rhcg*^{-/-} mice, this ammonium might be either shunted back into systemic circulation or not be absorbed at the level of the thick ascending limb.

Expression of NKCC2 was decreased in both *Rhcg*^{+/-} and *Rhcg*^{-/-} kidney tissues. NKCC2 is crucial for thick ascending limb NH₄⁺ absorption and concentration in the medulla. Thus, our results suggest that mechanisms contributing to create a high medullary ammonium concentration are altered in *Rhcg*-deficient mice. Other mechanisms such as increased removal of ammonium from the interstitium with venous blood might contribute also to the low medullary ammonium content. Metabolic acidosis alters concentrations of various vasoactive substances in the kidney, including higher levels of endothelin and prostaglandins and lower concentrations of NO (41, 42), which may alter medullary blood flow and the ability of the kidneys to maintain the cortico-papillary ammonium gradient.

RhCG Mediates NH₃ Transport Also at the Basolateral Side of CD Cells—Subcellular RhCG localization has remained controversial for many years (9, 10, 17). Here, we confirmed a strong labeling of both apical and basolateral poles of CD cells in mouse kidneys. These data were corroborated by our functional study on *in vitro* microperfused CCDs. We measured a 60% reduction in the NH₃ permeability at the basolateral side of

Incomplete dRTA in *Rhcg*-targeted Mice

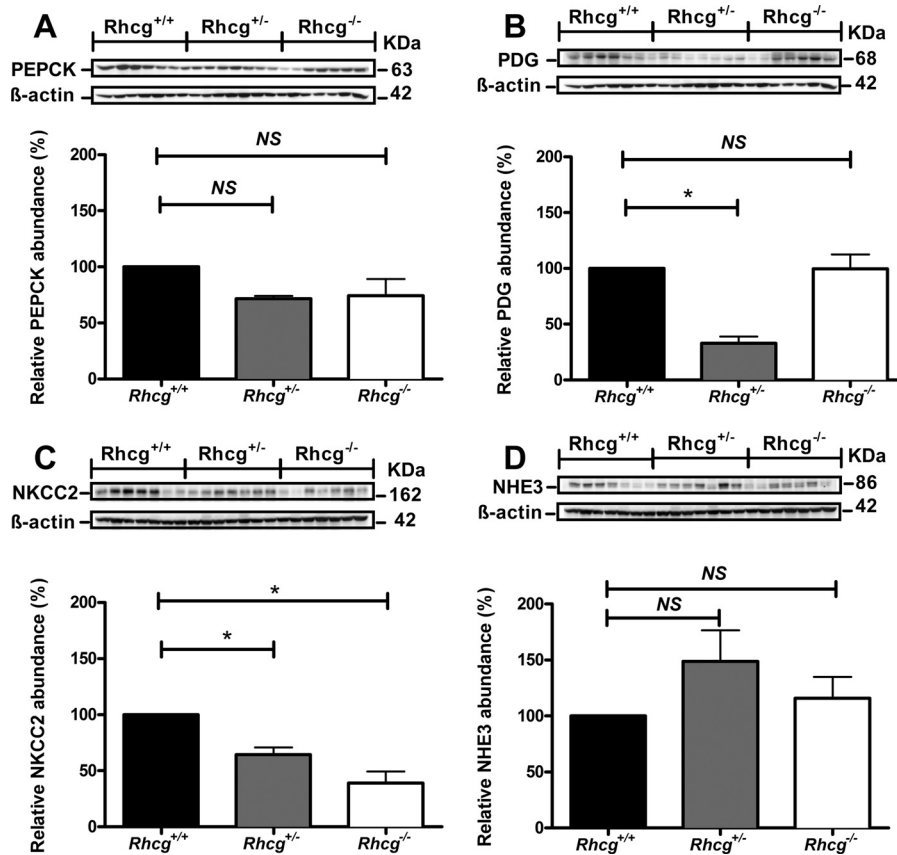


FIGURE 8. Deletion of *Rhcg* affects the abundance of proteins involved in ammoniogenesis and ammonium transport. Crude membrane and cytosolic fractions were prepared from total kidneys from *Rhcg*^{+/+}, *Rhcg*^{+/-}, and *Rhcg*^{-/-} mice after 2 days of HCl loading, 40 μ g loaded onto SDS-PAGE, and their abundance tested. A, PEPCK; B, PDG; C, the Na⁺-K⁺-2Cl⁻ cotransporter isoform 2 (NKCC2); and D, Na⁺/H⁺ exchanger isoform 3 (NHE3). All membranes were stripped and reprobed for β -actin to control for loading. Bar graphs summarize results from densitometric analysis of proteins of interest normalized against β -actin. *n* = 5 mice/genotype. * statistically significant, *p* < 0.05 versus *Rhcg*^{+/+} tissue. NS, not significant.

Rhcg^{-/-} CCD cells. This is the first evidence that Rhcg is also functional at the basolateral side of CDs cells and participates in basolateral NH₃ uptake. Previously, it has been assumed that basolateral uptake occurs mostly if not exclusively in the form of NH₄⁺ and that NH₃ plays no major role. Several pathways for NH₄⁺ uptake have been delineated from pharmacological and functional experiments that demonstrated a role for the Na⁺-K⁺-2Cl⁻ cotransporter NKCC1, the Na⁺/K⁺-ATPase, and possibly potassium channels where NH₄⁺ always would replace potassium (37, 38, 43). We performed our experiments in the absence of sodium to reduce NKCC1 and Na⁺/K⁺-ATPase activity, respectively. Thus, our experiments do not allow conclusions regarding the relative importance and contribution of these different pathways to total NH₃/NH₄⁺ uptake across the basolateral membrane, but they modify the current model of ammonium transport across the basolateral membrane. However it appears from the data on *Rhcg*^{+/-} CCD that apical NH₃ flux critically depends on full RhCG expression, whereas basolateral NH₃ flux is sustained with reduced RhCG expression suggesting that transport of the NH₃ form is most important at the apical side. Finally, our findings could also explain the complete lack or only mild phenotype observed in *Rhbg* knock-out mice (11, 44), where RhCG may have compensated for the lack of *RhBG*.

In summary, reduced expression or complete loss of expression of RhCG affects the ability of the kidneys to excrete acidic

urine and appropriately regulate acid/base homeostasis. We provide the first functional evidence for basolateral RhCG activity and show that RhCG is expressed and functional on apical and basolateral membranes of most cells lining the renal collecting duct. Thus, *Rhcg* haploinsufficiency or *Rhcg* deletion may contribute to orphan forms of inherited distal renal tubular acidosis in humans as well as to acquired forms of dRTA.

Acknowledgments—We thank Yves Colin and Isabelle Mourot-Chanteloup for fruitful discussions. We also thank Hanne Siedelmann for skillful technical assistance. The use of the Zurich Integrative Rodent Physiology Core Facility is gratefully acknowledged.

REFERENCES

- Hamm, L. L., Alpern, R. J., and Preisig, P. A. (2008) in *Seldin and Giebisch's The Kidney. Physiology and Pathophysiology* (Alpern, R. J., and Hebert, S. C., eds) pp. 1539–1585, Academic Press, New York
- Weiner, I. D., and Verlander, J. W. (2011) Role of NH₃ and NH₄⁺ transporters in renal acid-base transport. *Am. J. Physiol. Renal Physiol.* **300**, F11–F23
- Batlle, D. C., and Kurtzman, N. A. (1985) in *Renal Tubular Disorders* (Gonick, H. C., and Buckalew, V. M., eds) pp. 281–305, Marcel Dekker, Inc., New York
- Good, D. W. (1994) Ammonium transport by the thick ascending limb of Henle's loop. *Annu. Rev. Physiol.* **56**, 623–647
- Wagner, C. A., Devuyt, O., Belge, H., Bourgeois, S., and Houillier, P.

- (2011) The rhesus protein RhCG. A new perspective in ammonium transport and distal urinary acidification. *Kidney Int.* **79**, 154–161
6. Wagner, C. A., Devuyst, O., Bourgeois, S., and Mohebbi, N. (2009) Regulated acid-base transport in the collecting duct. *Pflugers Arch.* **458**, 137–156
 7. Wagner, C. A., Finberg, K. E., Breton, S., Marshansky, V., Brown, D., and Geibel, J. P. (2004) Renal vacuolar H⁺-ATPase. *Physiol. Rev.* **84**, 1263–1314
 8. DuBose, T. D., Jr., Good, D. W., Hamm, L. L., and Wall, S. M. (1991) Ammonium transport in the kidney: new physiological concepts and their clinical implications. *J. Am. Soc. Nephrol.* **1**, 1193–1203
 9. Quentin, F., Eladari, D., Cheval, L., Lopez, C., Goossens, D., Colin, Y., Cartron, J. P., Paillard, M., and Chambrey, R. (2003) RhBG and RhCG, the putative ammonia transporters, are expressed in the same cells in the distal nephron. *J. Am. Soc. Nephrol.* **14**, 545–554
 10. Brown, A. C., Hallouane, D., Mawby, W. J., Karet, F. E., Saleem, M. A., Howie, A. J., and Toye, A. M. (2009) RhCG is the major putative ammonia transporter expressed in the human kidney, and RhBG is not expressed at detectable levels. *Am. J. Physiol. Renal Physiol.* **296**, F1279–F1290
 11. Chambrey, R., Goossens, D., Bourgeois, S., Picard, N., Bloch-Faure, M., Leviel, F., Geoffroy, V., Cambillau, M., Colin, Y., Paillard, M., Houillier, P., Cartron, J. P., and Eladari, D. (2005) Genetic ablation of Rhbg in the mouse does not impair renal ammonium excretion. *Am. J. Physiol. Renal Physiol.* **289**, F1281–F1290
 12. Bishop, J. M., Verlander, J. W., Lee, H. W., Nelson, R. D., Weiner, A. J., Handlogten, M. E., and Weiner, I. D. (2010) *Am. J. Physiol. Renal Physiol.* **299**, F1065–F1077
 13. Biver, S., Belge, H., Bourgeois, S., Van Vooren, P., Nowik, M., Scohy, S., Houillier, P., Szpirer, C., Szpirer, C., Wagner, C. A., Devuyst, O., and Marini, A. M. (2008) A role for rhesus factor Rhcg in renal ammonium excretion and male fertility. *Nature* **456**, 339–343
 14. Lee, H. W., Verlander, J. W., Bishop, J. M., Igarashi, P., Handlogten, M. E., and Weiner, I. D. (2009) Collecting duct-specific Rh C glycoprotein deletion alters basal and acidosis-stimulated renal ammonia excretion. *Am. J. Physiol. Renal Physiol.* **296**, F1364–F1375
 15. Han, K. H., Lee, S. Y., Kim, W. Y., Shin, J. A., Kim, J., and Weiner, I. D. (2010) Expression of ammonia transporter family members, Rh B glycoprotein and Rh C glycoprotein, in the developing rat kidney. *Am. J. Physiol. Renal Physiol.* **299**, F187–F198
 16. Eladari, D., Cheval, L., Quentin, F., Bertrand, O., Mouro, I., Cherif-Zahar, B., Cartron, J. P., Paillard, M., Doucet, A., and Chambrey, R. (2002) Expression of RhCG, a new putative NH₃/NH₄⁺ transporter, along the rat nephron. *J. Am. Soc. Nephrol.* **13**, 1999–2008
 17. Kim, H. Y., Verlander, J. W., Bishop, J. M., Cain, B. D., Han, K. H., Igarashi, P., Lee, H. W., Handlogten, M. E., and Weiner, I. D. (2009) Basolateral expression of the ammonia transporter family member Rh C glycoprotein in the mouse kidney. *Am. J. Physiol. Renal Physiol.* **296**, F543–F555
 18. Jorgensen, K. (1957) Titrimetric determination of the net excretion of acid/base in urine. *Scand. J. Clin. Lab. Invest.* **9**, 287–291
 19. Nutbourne, D. M. (1961) The effect of dilution on the titratable acid in urine and acidified phosphate buffer solutions, and the correction for this effect in the determination of the rate of elimination of hydrogen ions from the body by the renal tubules. *Clin. Sci.* **20**, 263–278
 20. Seaton, B., and Ali, A. (1984) Simplified manual high performance clinical chemistry methods for developing countries. *Med. Lab. Sci.* **41**, 327–336
 21. Berthelot, M. (1859) Violet d'aniline. *Rep. Chim. App.* **1**, 284
 22. Curthoys, N. P., Kuhlenschmidt, T., Godfrey, S. S., and Weiss, R. F. (1976) Phosphate-dependent glutaminase from rat kidney. Cause of increased activity in response to acidosis and identity with glutaminase from other tissues. *Arch. Biochem. Biophys.* **172**, 162–167
 23. Hafner, P., Grimaldi, R., Capuano, P., Capasso, G., and Wagner, C. A. (2008) Pendrin in the mouse kidney is primarily regulated by Cl⁻ excretion but also by systemic metabolic acidosis. *Am. J. Physiol. Cell Physiol.* **295**, C1658–C1667
 24. Christensen, E. I., Nielsen, S., Moestrup, S. K., Borre, C., Maunsbach, A. B., de Heer, E., Ronco, P., Hammond, T. G., and Verroust, P. (1995) Segmental distribution of the endocytosis receptor gp330 in renal proximal tubules. *Eur. J. Cell Biol.* **66**, 349–364
 25. Marini, A. M., Matassi, G., Raynal, V., André, B., Cartron, J. P., and Cherif-Zahar, B. (2000) The human Rhesus-associated RhAG protein and a kidney homologue promote ammonium transport in yeast. *Nat. Genet.* **26**, 341–344
 26. Packer, R. K., Desai, S. S., Hornbuckle, K., and Knepper, M. A. (1991) Role of countercurrent multiplication in renal ammonium handling. Regulation of medullary ammonium accumulation. *J. Am. Soc. Nephrol.* **2**, 77–83
 27. Watts, B. A., 3rd, and Good, D. W. (1994) Apical membrane Na⁺/H⁺ exchange in rat medullary thick ascending limb. pH dependence and inhibition by hyperosmolality. *J. Biol. Chem.* **269**, 20250–20255
 28. Roos, A., and Boron, W. F. (1981) Intracellular pH. *Physiol. Rev.* **61**, 296–434
 29. Milton, A. E., and Weiner, I. D. (1998) Regulation of B-type intercalated cell apical anion exchange activity by CO₂/HCO₃⁻. *Am. J. Physiol.* **274**, F1086–F1094
 30. Flessner, M. F., Wall, S. M., and Knepper, M. A. (1992) Ammonium and bicarbonate transport in rat outer medullary collecting ducts. *Am. J. Physiol.* **262**, F1–F7
 31. Zhelyaskov, V. R., Liu, S., and Broderick, M. P. (2000) Analysis of nanoliter samples of electrolytes using a flow-through microfluorometer. *Kidney Int.* **57**, 1764–1769
 32. Hansen, G. M., Markesich, D. C., Burnett, M. B., Zhu, Q., Dionne, K. M., Richter, L. J., Finnell, R. H., Sands, A. T., Zambrowicz, B. P., and Abuin, A. (2008) Large-scale gene trapping in C57BL/6N mouse embryonic stem cells. *Genome Res.* **18**, 1670–1679
 33. Verlander, J. W., Miller, R. T., Frank, A. E., Royaux, I. E., Kim, Y. H., and Weiner, I. D. (2003) Localization of the ammonium transporter proteins RhBG and RhCG in mouse kidney. *Am. J. Physiol. Renal Physiol.* **284**, F323–F337
 34. Kim, H. Y., Verlander, J. W., Bishop, J. M., Cain, B. D., Han, K. H., Igarashi, P., Lee, H. W., Handlogten, M. E., and Weiner, I. D. (2009) *Am. J. Physiol. Renal Physiol.* **296**, F1364–F1375
 35. Kikeri, D., Sun, A., Zeidel, M. L., and Hebert, S. C. (1989) Cell membranes impermeable to NH₃. *Nature* **339**, 478–480
 36. Bleich, M., Köttgen, M., Schlatter, E., and Greger, R. (1995) Effect of NH₄⁺/NH₃ on cytosolic pH and the K⁺ channels of freshly isolated cells from the thick ascending limb of Henle's loop. *Pflugers Arch.* **429**, 345–354
 37. Wall, S. M., and Koger, L. M. (1994) NH₄⁺ transport mediated by Na⁺-K⁺-ATPase in rat inner medullary collecting duct. *Am. J. Physiol.* **267**, F660–F670
 38. Wall, S. M., and Fischer, M. P. (2002) Contribution of the Na⁺-K⁺-2Cl⁻ cotransporter (NKCC1) to transepithelial transport of H⁺, NH₄⁺, K⁺, and Na⁺ in rat outer medullary collecting duct. *J. Am. Soc. Nephrol.* **13**, 827–835
 39. Gruswitz, F., Chaudhary, S., Ho, J. D., Schlessinger, A., Pezeshki, B., Ho, C. M., Sali, A., Westhoff, C. M., and Stroud, R. M. (2010) Function of human Rh based on structure of RhCG at 2.1 Å. *Proc. Natl. Acad. Sci. U.S.A.* **107**, 9638–9643
 40. Mouro-Chanteloup, I., Cochet, S., Chami, M., Genetet, S., Zidi-Yahiaoui, N., Engel, A., Colin, Y., Bertrand, O., and Ripoché, P. (2010) Functional reconstitution into liposomes of purified human RhCG ammonia channel. *PLoS ONE* **5**, e8921
 41. Jones, E. R., Beck, T. R., Kapoor, S., Shay, R., and Narins, R. G. (1984) Prostaglandins inhibit renal ammoniogenesis in the rat. *J. Clin. Invest.* **74**, 992–1002
 42. Prabhakar, S. S. (2004) Regulatory and functional interaction of vasoactive factors in the kidney and extracellular pH. *Kidney Int.* **66**, 1742–1754
 43. Wall, S. M., Fischer, M. P., Kim, G. H., Nguyen, B. M., and Hassell, K. A. (2002) In rat inner medullary collecting duct, NH uptake by the Na,K-ATPase is increased during hypokalemia. *Am. J. Physiol. Renal Physiol.* **282**, F91–F102
 44. Bishop, J. M., Verlander, J. W., Lee, H. W., Nelson, R. D., Weiner, A. J., Handlogten, M. E., and Weiner, I. D. (2010) Role of the Rhesus glycoprotein, Rh B glycoprotein, in renal ammonia excretion. *Am. J. Physiol. Renal Physiol.* **299**, F1065–F1077